

In situ synthesis of hydroxyapatite nanorods on graphene oxide nanosheets and their reinforcement in biopolymer scaffold

Cijun Shuai^{a,b,c}, Bo Peng^a, Pei Feng^{a,*}, Li Yu^a, Ruilin Lai^d, Anjie Min^e

^aState Key Laboratory of High Performance Complex Manufacturing, College of Mechanical and Electrical Engineering, Central South University, Changsha 410083, China

^bInstitute of Bioadditive Manufacturing, Jiangxi University of Science and Technology, Nanchang 330013, China

^cShenzhen Institute of Information Technology, Shenzhen 518172, China

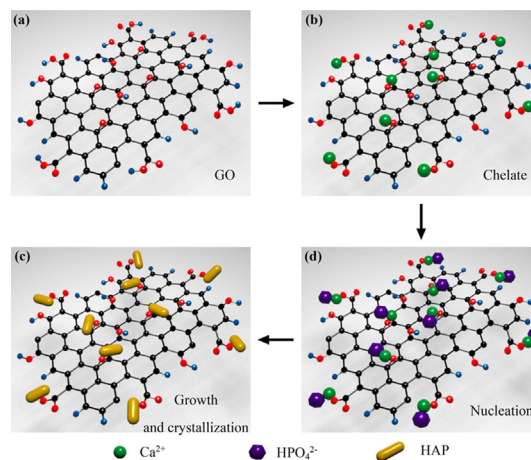
^dState Key Laboratory of Powder Metallurgy, Central South University, Changsha 410083, China

^eDepartment of Oral and Maxillofacial Surgery, Center of Stomatology, Xiangya Hospital, Central South University, Changsha 410078, China

HIGHLIGHTS

- GO was employed to in situ synthesize GO-HAP via hydrothermal reaction.
- GO-HAP was blended with PLLA to fabricate biopolymer scaffold via SLS.
- Uniformly decorated HAP on GO was about 5 nm in diameter and 60 nm in length.
- The addition of GO-HAP enhanced compressive strength and modulus of PLLA scaffold.
- The PLLA/GO-HAP scaffold displayed good bioactivity and favorable cytocompatibility.

GRAPHICAL ABSTRACT



ARTICLE INFO

Article history:

Received 3 December 2020

Revised 13 March 2021

Accepted 20 March 2021

Available online 5 April 2021

Keywords:

In situ synthesis

GO

HAP

Mechanical properties

Bioactivity

ABSTRACT

Introduction: It is urgently needed to develop composite bone scaffold with excellent mechanical properties and bioactivity in bone tissue engineering. Combining graphene oxide (GO) and hydroxyapatite (HAP) for the reinforcement of biopolymer bone scaffold has emerged as a promising strategy. However, the dispersion of GO and HAP remains to be a big challenge.

Objectives: In this present work, the mechanical properties of GO and the bioactivity of and HAP were combined respectively via in situ synthesis for reinforcing biopolymer bone scaffold.

Methods: GO nanosheets were employed to in situ synthesize GO-HAP nanocomposite via hydrothermal reaction, in which their abundant oxygen-containing groups served as anchor sites for the chelation of Ca^{2+} and then Ca^{2+} absorbed HPO_4^{2-} via electrovalent bonding to form homogeneously dispersed HAP nanorods. Thereby, the GO-HAP nanocomposite was blended with biopolymer poly-L-lactic acid (PLLA) for fabricating biopolymer scaffold by selective laser sintering (SLS).

Results: GO nanosheets were uniformly decorated with HAP nanorods, which were about 60 nm in length and 5 nm in diameter. The compressive strength and modulus of PLLA/12%GO-HAP were significantly increased by 53.71% and 98.80% compared to the pure PLLA scaffold, respectively, explained on the base of pull out, crack bridging, deflection and pinning mechanisms. Meanwhile, the mineralization

Peer review under responsibility of Cairo University.

* Corresponding author.

E-mail address: fengpei@csu.edu.cn (P. Feng).

<https://doi.org/10.1016/j.jare.2021.03.009>

2090-1232/© 2021 The Authors. Published by Elsevier B.V. on behalf of Cairo University.

This is an open access article under the CC BY-NC-ND license (<http://creativecommons.org/licenses/by-nc-nd/4.0/>).

experiments indicated the PLLA/GO-HAP scaffold displayed good bioactivity by inducing the formation of apatite layer. Besides, cell culturing experiments demonstrated the favorable cytocompatibility of scaffold by promoting cell adhesion and proliferation.

Conclusions: The present findings show the potential of PLLA/GO-HAP composite scaffold via in situ synthesis in bone tissue engineering.

© 2021 The Authors. Published by Elsevier B.V. on behalf of Cairo University. This is an open access article under the CC BY-NC-ND license (<http://creativecommons.org/licenses/by-nc-nd/4.0/>).

Introduction

Graphene oxide (GO), as an oxidized form of graphene sheets, has attracted tremendous attention in reinforcing biopolymer because of the excellent mechanical properties [1–3]. It can form strong interfacial interactions with biopolymer matrix [4,5], and provide reactive sites for generating new composites with superior properties as compared to their individual components on account of the presence of plentiful oxygen functional groups [6–8]. Hydroxyapatite (HAP), as a calcium phosphate, possesses excellent bioactivity and osteoconductivity because of its chemical composition similarity to natural bone [9–11]. Meanwhile, it has been usually used as a mechanical reinforcement phase for biopolymer, while the reinforcing effect of HAP is not to be compared with that of GO resulted from its intrinsic brittleness [12–14]. Hence, the combination of GO and HAP will show great potential for the reinforcement of biopolymer due to their superiority in mechanical properties, bioactivity and osteoconductivity.

Recently, some strategies including solution blending, chemical grafting and so on have been implemented in combining GO and HAP for the reinforcement of biopolymer. Bhahat et al. applied solution blending to introduce GO and HAP into collagen and fabricated Col/GO/HAP nanocomposite scaffold via freeze drying, and found that the compressive stress and biocompatibility were improved [15]. Renet al. implemented solution blending to introduce GO and HAP into poly (L-lactic-co-glycolic acid) (PLGA) and fabricated PLGA/GO/HAP nanofibre scaffold via electrospinning, and discovered that the tensile strength and cytocompatibility were improved [16]. Xiong et al. treated HAP with glucosamine and then blended it with GO and sodium alginate (SA) to fabricate GO/HAP/SA nanocomposite scaffold through freeze drying, and found that the compressive properties and bioactivity of the scaffold were better than those of neat SA scaffold [17]. The above methods introduced GO and HAP into biopolymer, however, to the best of our knowledge, the dispersion of GO and HAP remained a challenge.

In situ synthesis provided a potentially attractive strategy to synthesize GO-based nanocomposites with good dispersion and interfacial bonding as in this method the stacking of GO nanosheets can be reduced by the grown inorganic phase, and the powerful bonding between inorganic phase and GO nanosheets can be obtained by the nucleation and growth of nanocrystals [18–20]. Previous reports have demonstrated that the abundant mineralization related groups (epoxide, and carboxylic groups) on GO surface can act as effective nucleation sites for precipitating Ca^{2+} , and then regulate the nucleation and growth process of HAP nanocrystals [21,22]. The HAP nanocrystals can form tight interfacial bonding with GO nanosheets and distribute homogeneously on the surface of GO nanosheets thus avoiding their aggregation [23–25].

In this present work, GO nanosheets were employed to in situ synthesis HAP via hydrothermal reaction with the assistance of calcium and phosphorus precursors. The GO-HAP nanocomposite was introduced into biopolymer PLLA, and selective laser sintering (SLS) was employed to fabricate porous PLLA/GO-HAP bone scaffold. The phase composition and microstructure of GO-HAP nanocomposite were analyzed to study the in situ growth. The

compressive properties of the scaffold were investigated, and the crack propagation mechanisms were discussed. Meanwhile, the bioactivity was assessed by simulated body fluid (SBF) immersion test and the apatite forming ability was investigated by studying the morphology and element composition. Besides, the cytocompatibility was analyzed by studying cell adhesion and proliferation.

Materials and methods

Reagents and materials

GO with product number TNG-10 was provided by Chengdu Organic Chemicals Co., Ltd. of Chinese Academy of Sciences. Ammonia solution (NH_4OH), diammonium hydrogen phosphate ($(\text{NH}_4)_2\text{HPO}_4$) and calcium nitrate tetrahydrate ($\text{Ca}(\text{NO}_3)_2 \cdot 4\text{H}_2\text{O}$) were provided by Sinopharm Chemical Reagent Co., Ltd. PLLA powders with a molecular weight of 150 kDa were obtained from Shenzhen Polymtek Biomaterial Co., Ltd.

In situ synthesis of GO-HAP composite powders

Synthesis of GO-HAP composite powders was presented in Fig. 1(a). In detail: A certain amount of GO was added in deionized water, and a uniform light-yellow suspension was obtained by ultrasonic treatment, indicating that GO was uniformly exfoliated into flakes. $\text{Ca}(\text{NO}_3)_2 \cdot 4\text{H}_2\text{O}$ and $(\text{NH}_4)_2\text{HPO}_4$ were used as precursors of calcium and phosphorus to in situ synthesize HAP, respectively. The molar ratio of calcium and phosphorus in the experiment was controlled at 1.67, which was consistent with the molar ratio of calcium and phosphorus in human bone components. $\text{Ca}(\text{NO}_3)_2 \cdot 4\text{H}_2\text{O}$ was sufficiently dissolved in deionized water and then added to the above mentioned GO suspension. The pH was controlled at 10 using ammonia water, and magnetically stirred for 1 h under a water bath at 50 °C to promote sufficient reaction between Ca^{2+} and the functional groups of GO. $(\text{NH}_4)_2\text{HPO}_4$ was slowly added to the GO- Ca^{2+} system with continuous stirring, and the mixed solution further reacted at 60 °C for 6 h, while pH was controlled above 10 with ammonia water. Thereafter, the mixed solution was aged in an environment of 50 °C for 1 d. After centrifugation, the precipitates were repeatedly rinsed five times, and GO-HAP composite powders were obtained after drying.

Fabrication of scaffolds

PLLA/GO-HAP composite powders were fabricated through the following steps, as presented in Fig. 1(b). The powders mixed in different proportions were respectively added in deionized water, and then 30 min of ultrasonic treatment was performed. The obtained solution was continuously stirred in 50 °C environment for 2 h, and then poured into a centrifuge tube and centrifuged continuously at a speed of 6000 r/min for 8 min. The precipitates were collected and dried overnight to obtain composite powders. According to different mass fraction ratios of 100:0, 96:4, 92:8, 88:12 and 84:16, different ratios of composite powders were pre-

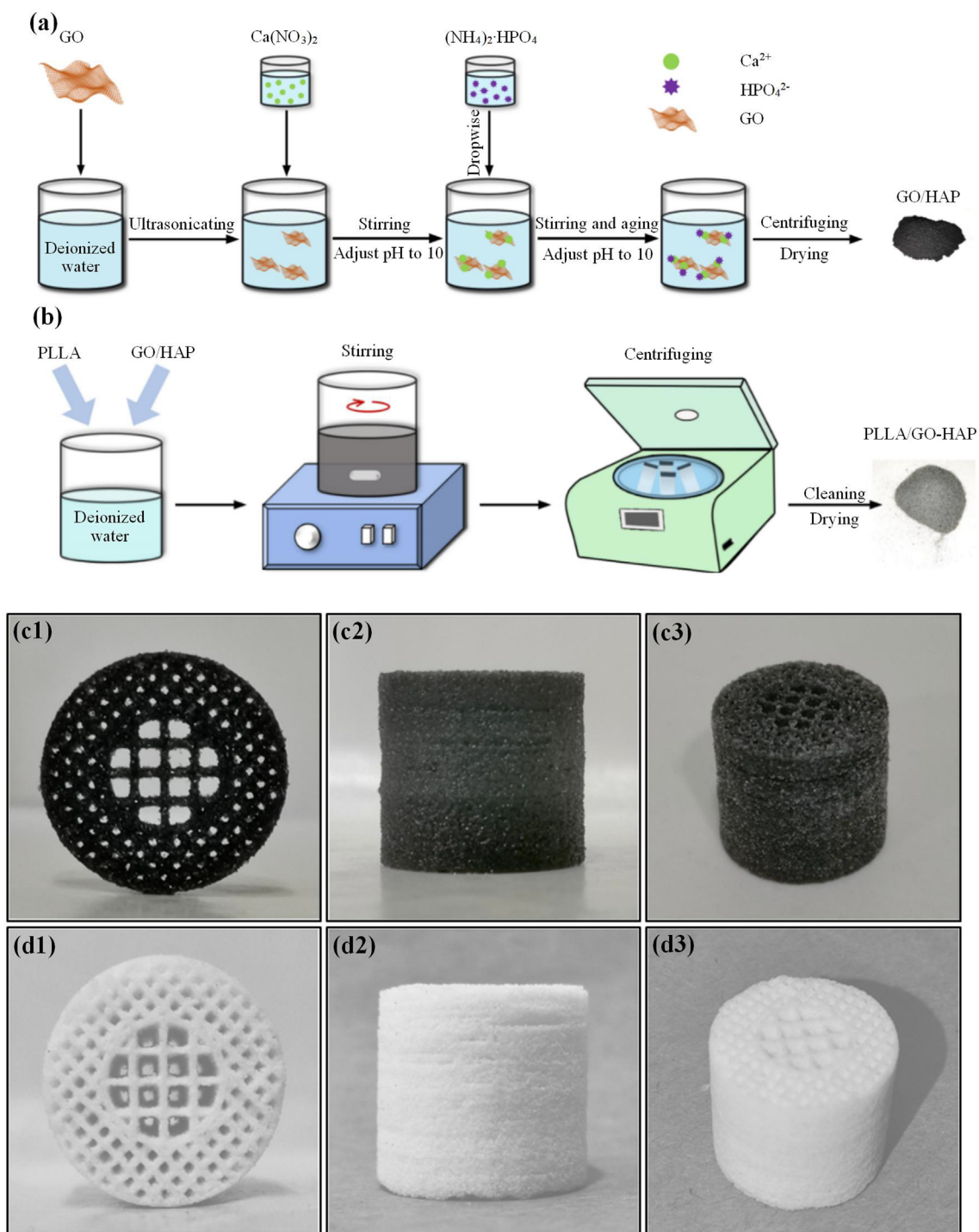


Fig. 1. Schematic diagram of the preparation of GO-HAP composite powders via in situ synthesis (a), the preparation of PLLA/GO-HAP composite powders (b), the three orthographic views of the PLLA/GO-HAP (c) and PLLA (d) scaffolds.

pared and defined as PLLA, PLLA/4%GO-HAP, PLLA/8%GO-HAP, PLLA/12%GO-HAP and PLLA/16%GO-HAP, respectively.

An SLS system with CO₂ laser, 3D galvanometer scanner and computer-control system was used to fabricate the PLLA and PLLA/GO-HAP scaffolds. The specific process was as follows: The 3D model of the scaffold was drawn in a computer with 3D drawing software and imported into the control system. The composite powders were evenly spread on the workbench, and then a laser beam sintered powder layer based on the slicing data of the 3D model. Afterward, the workbench declined a height of sintered layer, and a new layer of composite powders was spread. After

repeated layers of powdering and sintering, a porous scaffold with the size of $\Phi 15 \text{ mm} \times 15 \text{ mm}$ was finally formed, as presented in Fig. 1(c, d).

Characterization

The micromorphology analysis of the composite powders was performed using a transmission electron microscope (TEM, FEI) at an accelerating voltage of 100 kV. A drop of GO-HAP composite suspension (the solution was formed by dispersing GO-HAP in deionized water) was dropped onto copper grids, and then dried

to prepare the specimens for TEM imaging. The morphology and element composition were evaluated with a Phenom ProX scanning electron microscope (SEM) and an energy dispersive spectrometer (EDS) (PhenomWorld BV) at an accelerating voltage of 15 kV. In the case of SEM, the specimens were sputter-coated with a thin film of gold before the examination.

To study the functional groups of the composition powders, Fourier transform infrared (FTIR) spectra were recorded via spectrophotometer (Changsha Tianheng Scientific Instrument Equipment Co., Ltd.) ranging from 400 to 4000 cm^{-1} , with a resolution of 2 cm^{-1} using a KBr pellet method. Raman spectra were recorded using micro-Raman spectroscopy, the specimens were excited by a laser source with a wavelength of 532 nm. The phase composition of the fabricated scaffolds and powders was investigated using X-ray diffraction (XRD) diffractometer (New Empyrean Co., Ltd.) using $\text{Cu-K}\alpha$ radiation at 40 mA and 40 kV. Scanning was performed with 2θ values ranging from 5 to 80° at a rate of 8°/min.

Mechanical properties, wettability and thermal properties

According to the American Society for Testing and Materials (ASTM) D6641 standard, compression properties were evaluated with a mechanical testing machine (Ji'nan Zhongluchang Testing Machine Manufacturing Co., Ltd.) at room temperature. The scaffold specimen size was $\Phi 5 \text{ mm} \times 7 \text{ mm}$, and the crosshead speed was set to 0.5 mm/min. A compressive load was applied to the specimen continuously until it was completely destroyed. The compression test sensor recorded the stress-strain curves of this process at the meantime. The compressive strength and modulus were computed from the strain-stress curve. The compressive modulus of the specimen was calculated from the slope of the initial elastic deformation stage of the curve, and the compressive strength was calculated by the ratio of the peak load to the cross-sectional area of the specimen. Each ratio was tested five times, and the average of which was computed to determine final result.

Contact angle experiments were performed with an attention theta lite optical tensiometer (Biolin Scientific Co., Ltd.). Specimens with a size of $10 \times 10 \times 2 \text{ mm}^3$ were placed on the experimental workbench. A drop of distilled water was added to the specimen surface by a microinjector, and the measurement was performed within 10 s. The contact angles of 6 random contact test points per specimen were studied. Thermal properties were evaluated using a thermogravimetric analysis (Nanjing Dazhan Electromechanical Technology institute). About 8 mg of the composites were enclosed in ceramic crucible, and then heated from room temperature to 500 °C at a rate of 10 °C/min under nitrogen atmosphere. The thermogravimetric analysis (TGA) and differential scanning calorimetry (DSC) curves of the composites at 50–500 °C were measured to investigate the thermal stability. The 300–450 °C range on the TGA curve was enlarged to better observe the main mass loss stage. After fitting the polynomial to the data of TGA, the derivative thermogravimetry (DTG) curves were obtained by calculating the first derivative of the polynomial.

Mineralization experiment

To assess the bioactivity, the scaffolds were immersed into SBF for 28 d. After the period, the scaffolds were separated from SBF solution, and then cleaned with deionized water and dried. The morphology of scaffolds after the test was visualized by SEM, and the element composition of apatite layer was carried out by EDS.

Cytocompatibility

Scaffolds were sterilized under UV-light for 1 h and then located in the 12-well plate. MG-63 were seeded (50000 cells/scaffold) into

scaffolds and incubated in Dulbecco's modified Eagle's medium (DMEM) supplemented with 10% fetal calf serum and 1% antibiotic. They were cultured for 1, 3 and 5 d in a humidified atmosphere.

The cell seeded scaffolds were washed gently in phosphate buffered solution (PBS) after the stipulated time. For determining the cell morphology, the specimens were fixed with 2.5% glutaraldehyde. Subsequently, the cells on the scaffolds were allowed to dehydrate for about 10 m each in a graded ethanol series and dried in air. Finally, the cell seeded scaffolds were sputtered with platinum and then observed using SEM. For evaluating cell viability, the specimens were stained for 30 m with 15 $\mu\text{g mL}^{-1}$ calcein AM, and then were analyzed via fluorescence microscopy (Olympus Corporation, Tokyo, Japan). In detail, the live cells were green in the obtained images.

Statistical analysis

All the data were presented as mean \pm standard deviation, and SPSS version 19 (IBM Co.) was employed to assess statistical significance. Labels *, ** and *** represented $P < 0.05$, $P < 0.01$ and $P < 0.001$, respectively.

Results and discussion

GO, GO-HAP composite powders

Raman spectra of GO and GO-HAP were presented in Fig. 2(a). Compared to that of GO, the spectrum of GO-HAP possessed a peak at 964 cm^{-1} , which was attributed to non-degenerated symmetric stretching vibration of PO_4^{3-} group [5]. Typical D and G bands of GO were appeared at 1335 and 1586 cm^{-1} , respectively [26]. The D and G bands for GO-HAP were located at 1345 and 1593 cm^{-1} , respectively. The red-shift could be attributed to the physical or chemical mutual effect between GO lattice and HAP nanocrystallines [20,27]. The I_D/I_G value of GO was 1.15, while the I_D/I_G value of GO-HAP was 1.11, as displayed in Fig. 2(a). The slight decrease in I_D/I_G value represented the decrease of defect density in GO. It could be well documented that due to the partial reduction process resulting from the hydrothermal reaction of in situ synthesis, the oxygen functional groups on GO sheets could be removed and the conjugated graphene network (sp^2 carbon) would be reestablished by the formation of double bonds [28]. To further identify the functional groups of synthesized composite powders, FTIR analysis was performed, as displayed in Fig. 2(b). Typical transmittance bands of GO at 3398, 1735 and 1622 cm^{-1} were ascribed to —OH stretching, the stretching vibration of —C=O and the stretching vibration of aromatic C=C, respectively [29]. As to the spectrum of GO-HAP, the stretching mode and librational mode of the structural —OH which appeared at 3569 and 632 cm^{-1} were not clearly observed, and the intensity of the peak for —C=O decreased. These changes indicated the formation of reduced GO in the GO-HAP composite powders after hydrothermal treatment [30]. Furthermore, the bands at 1099 and 1033 cm^{-1} represented the asymmetric stretching vibrations of P-O in PO_4^{3-} groups, while the bands at 568 and 601 cm^{-1} were ascribed to the bending vibrations of O-P-O in PO_4^{3-} groups [4]. The vibrations of PO_4^{3-} groups proved the possible formation of HAP in the GO-HAP composite, which was consistent with Raman analysis. The XRD patterns presented in Fig. 2(c) confirmed the crystalline nature of GO and GO-HAP. The sharp characteristic peak at $2\theta = 10.9^\circ$ was attributed to the (001) plane of GO. The Bragg reflection peaks at 2θ values of 26.0°, 32.0°, 33.0°, 34.2°, 40.0°, 46.8°, 49.5° and 53.3° corresponded to the (002), (211), (112), (300), (310), (222), (213) and (004) diffraction planes of HAP, respectively, agreed quite well with the JCPDS card (No. 09e0432) [10]. Meanwhile, the intact diffraction

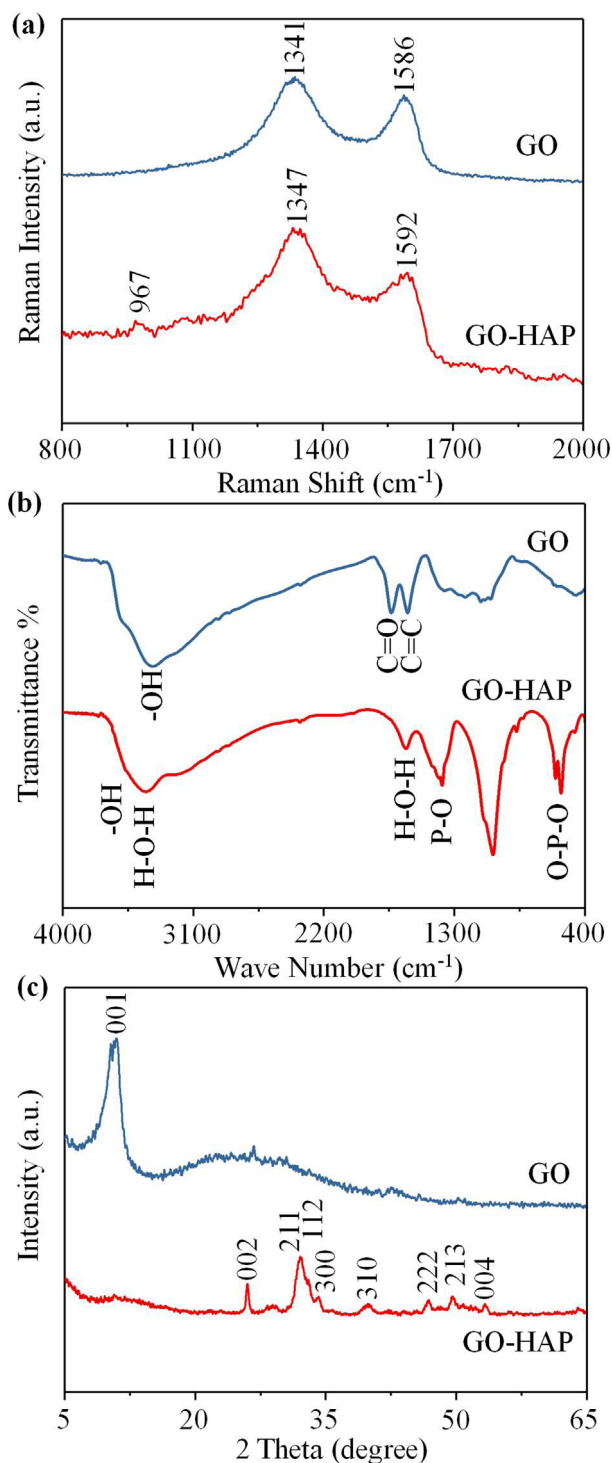


Fig. 2. Raman spectra (a), FTIR spectra (b) and XRD spectra (c) of GO and GO-HAP.

peaks indicated that the obtained HAP particles were nano crystals, which had been suggested to have excellent osseointegration properties and to be easier to be embedded into the GO nanosheets [11,21]. The synthesized GO-HAP composite powders displayed the similar diffraction peaks as those of the GO and HAP. Thus, considering the results of FTIR, Raman and XRD, the successful formation of HAP on the surface of GO was demonstrated by the chemical characterization.

The surface properties of GO and GO-HAP powders were demonstrated by using SEM, EDS and TEM as shown in Fig. 3.

The images in Fig. 3(a, c) displayed the folds and scrolls at the rim of the GO, which would be beneficial for the mechanical interlocking as well as the adhesion with the HAP [22]. Meanwhile, GO possessed a high specific surface area, which could effectively enhance the loading levels of the HAP [21,31]. The surface morphology of GO-HAP composite powders presented in Fig. 3(d) demonstrated a rough structure with many cluster-like granules. Besides, the uniform element mapping distribution of C (Fig. 3(b)) and Ca (Fig. 3(e)) elements implied that the HAP nanorods were uniformly dispersed in the GO matrix. This result was further confirmed by TEM, which illustrated a homogeneous dispersion of HAP nanorods onto GO nanosheets as well as the sheet edges as shown in Fig. 3(f). Moreover, the HAP nanorods possessed a typical rod-like shape, the nanometric size of which was about 60 nm in length and 5 nm in diameter.

The formation mechanism of HAP nanorods on GO nanosheets was demonstrated in Fig. 4. GO nanosheets possessed abundant oxygen-containing groups including hydroxyl, epoxy, carboxyl and carbonyl groups [4,5,32], which acted as anchor sites that induced the in situ growth of HAP nanorods on GO nanosheets [25,33]. In the initial stage, Ca^{2+} was added to the sonicated GO solution to chelate with the oxygen atoms of the epoxy groups as well as the carbonyl groups. Then, HPO_4^{2-} , formed by the dissolution of Na_2HPO_4 under an alkaline environment, reacted with Ca^{2+} via electrovalent bonds [5,20,34]. Therefore, a large number of HAP nuclei was formed and uniformly distributed on the GO nanosheets under stirring condition. As a result, the HAP nuclei gradually crystallized and grown into nanorods in a hydrothermal environment.

Properties of scaffolds

The morphologies of GO-HAP in the polymer matrix were observed by SEM (Fig. 5). Compared with the flat surface of the pure PLLA, the PLLA/GO-HAP scaffolds with 4%, 8% and 12% mass fractions of GO-HAP appeared well dispersed white particles. Among them, white sheets corresponding to GO were observed on the scaffolds added with 8% and 12% GO-HAP, which was also consistent with previous studies [35]. When the mass fraction continued to increase to 16%, large amounts of aggregation were formed, and even apparently continuous phases appeared, indicating that the dispersion was poor under this proportion of load. In previous study, GO and HAP were prone to agglomeration when they were mixed with polymers [36,37]. GO tended to form irreversible agglomerates in the polymer matrix due to the strong van der Waals force among them, and the aggregation of HAP nanoparticles in the polymer matrix was ascribed to high surface energy as well as large surface area [36,38]. However, for the GO-HAP nanocomposite produced by the in situ growing method, HAP nanorods uniformly grew on the surface of GO [22]. By being inserted into the nanosheets of GO, HAP reduced its stacking [39]. Therefore, HAP nanorods and GO nanosheets formed a synergistic system that supported each other to reduce agglomeration and promoted dispersion.

The compressive properties of the scaffolds including compressive strength and modulus were shown in Fig. 6. GO and HAP as the additive phases could enhance the mechanical properties of the polymer to a certain extent, which explained that the mechanical properties of composite scaffolds were improved compared to the pure PLLA scaffold [4,25]. Among them, the PLLA/12%GO-HAP scaffold had the highest strength and modulus, which were 21.52 MPa and 4.99 GPa, respectively. For the PLLA/16%GO-HAP scaffold, the compressive strength and modulus decreased slightly to 19.00 MPa and 4.90 GPa, respectively. Their dispersion in the polymer matrix was also a key factor affecting mechanical properties [40,41]. Although GO-HAP content was

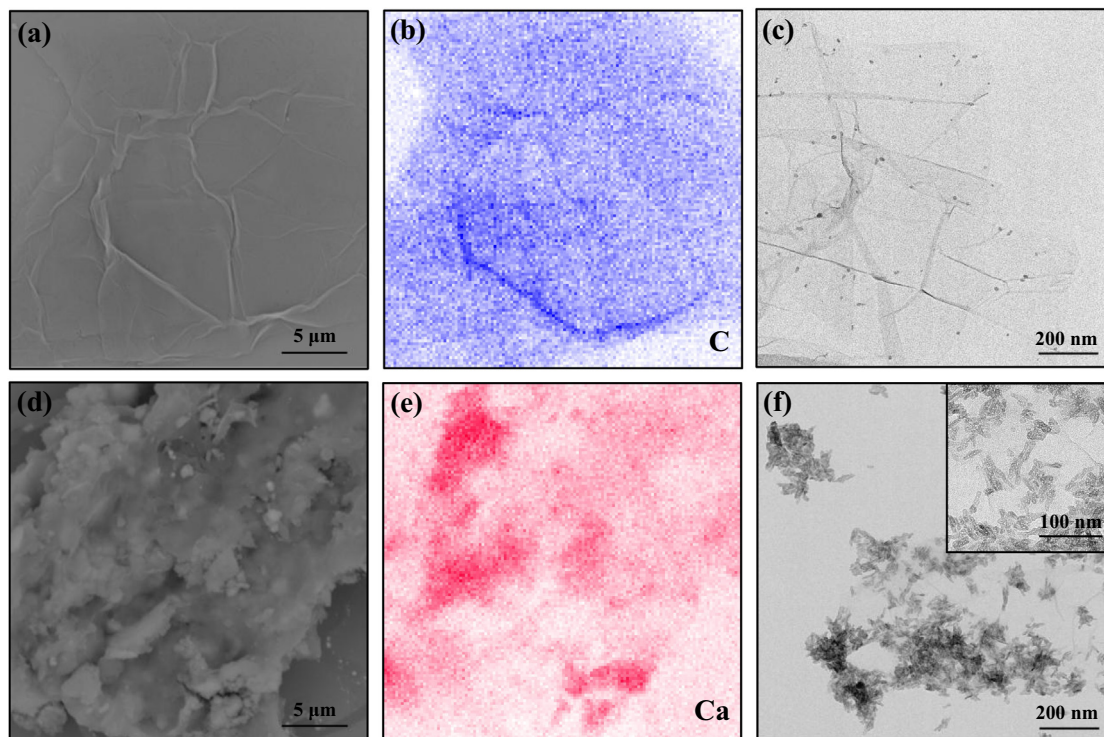


Fig. 3. SEM morphologies (a, d) and the corresponding EDS mapping images (b, e), TEM images (c, f) of GO (a-c) and GO-HAP (d-f) powders.

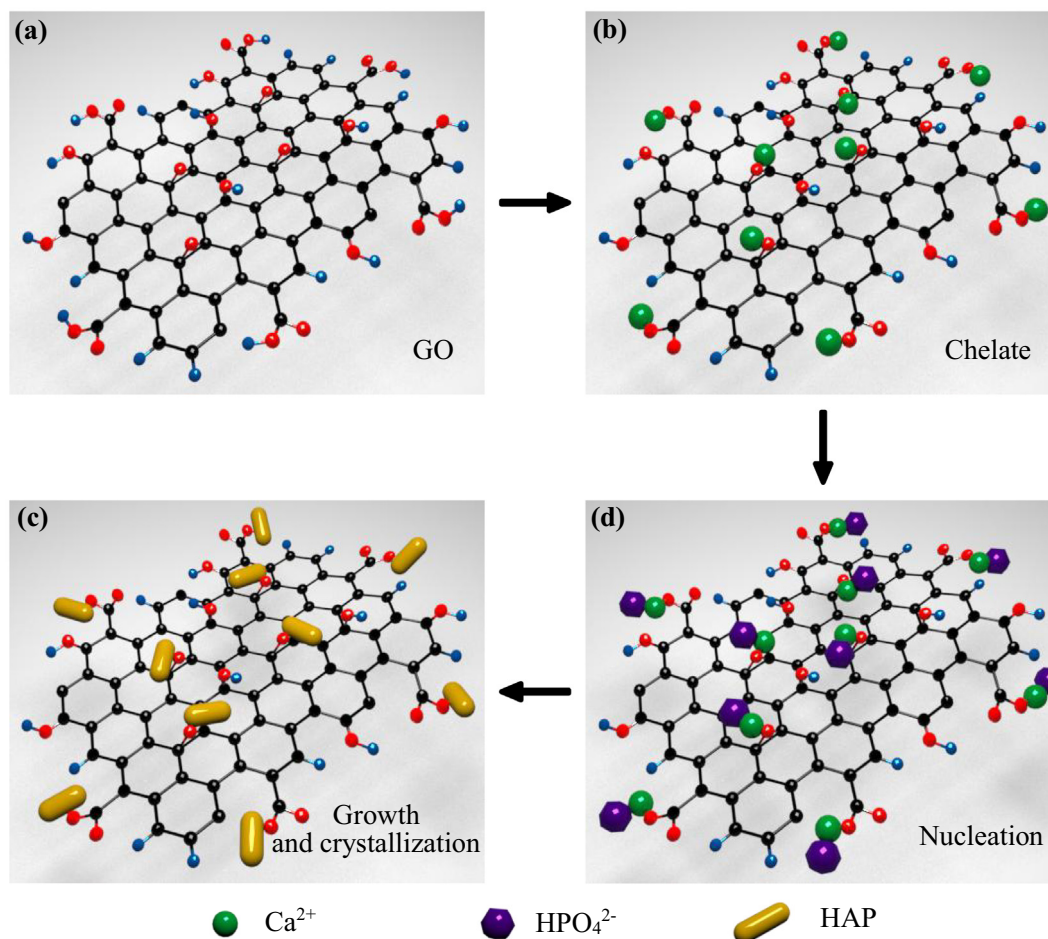


Fig. 4. In situ grown mechanism of HAP nanorods on GO nanosheets: pure GO nanosheets (a), chelation of Ca^{2+} with GO nanosheets (b), growth and crystallization of HAP nanorods (c), nucleation of HAP (d).

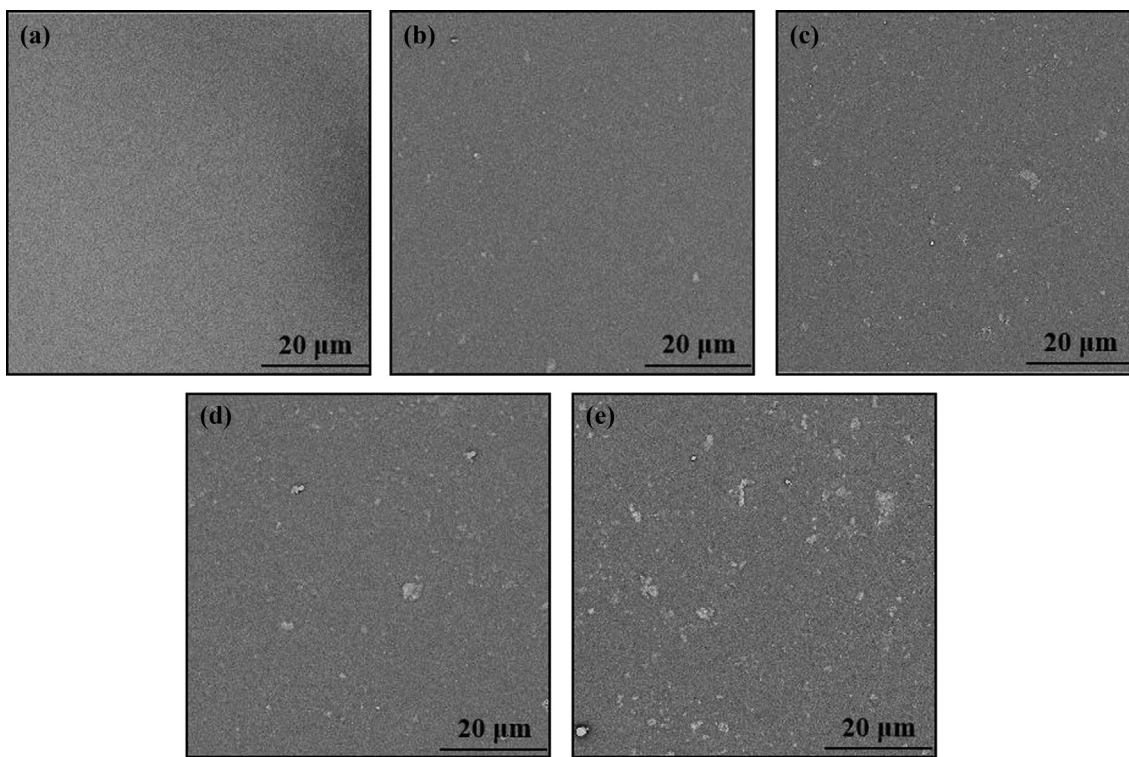


Fig. 5. Morphologies of the pure PLLA scaffold (a), and the PLLA/GO-HAP scaffolds with 4% (b), 8% (c), 12% (d) and 16% (e) mass fractions of GO-HAP.

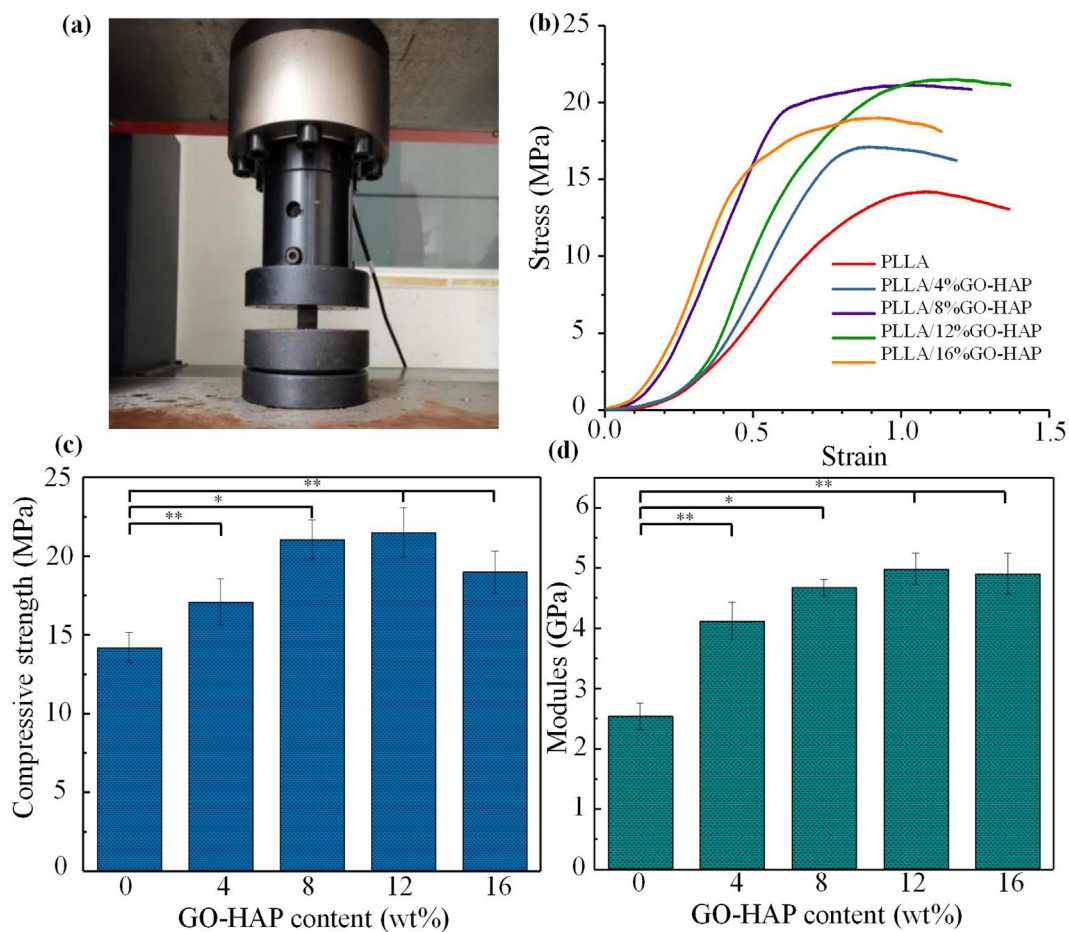


Fig. 6. Compressive properties of the pure PLLA and PLLA/GO-HAP scaffolds: compression testing image (a), stress-strain curves (b), variation of compressive strength (c), variation of compressive modulus (d).

the highest, the compression performance of PLLA/16%GO-HAP scaffold decreased due to the poor dispersion as previously described. Therefore, as the mass fraction increased, the mechanical properties of the scaffold firstly increased and then decreased [42].

The crack propagation morphologies in the scaffolds were observed by SEM, as presented in Fig. 7(a-d). It could be observed that the crack bridging, pull out, crack deflection, crack pinning hindered the crack propagation. The corresponding crack extension models were proposed, as presented in Fig. 7(e). Crack bridging appeared when GO-HAP connected the crack interfaces in the crack wake. On the other hand, when fracture occurred in the scaffolds, GO-HAP might be pulled out from the PLLA matrix. Cracks generally expanded in one direction without deflection during extension [43]. When the crack encountered the GO-HAP nanocomposite, it would be forced to veer off the original course due to tilt and torsion, or be pinned. The above effects would induce the cracks to consume more energy when it propagated, thus enhancing the mechanical properties [4].

Bioactivity, the ability to form bone-like apatite layer, was an important character of bone scaffold [11,44]. Apatite phase formed on the PLLA/GO-HAP scaffolds after immersed in SBF for 28 d were investigated by SEM, as shown in Fig. 8 (a-h). It could be observed that clustered dandelion-like apatite deposited on the scaffolds,

while the area of apatite layer became larger with the proportion of GO-HAP increased. To identify the chemical compositions of the deposits, EDS was conducted on the scaffolds as shown in Fig. 8 (i-l). According to the EDS spectra, the elements were mainly C, O, Ca and P. Meanwhile, the Ca/P ratio of the deposits increased from 1.47 to 1.65 as the GO-HAP mass fraction increased from 4% to 16%, which were gradually close to the 1.67 of HAP [10]. The results revealed that the PLLA/GO-HAP scaffolds owned well bioactivity to induce bone-like apatite layer, which was vital to form a chemical bond between the implant scaffold and living bone tissue [13,45]. Previous studies had demonstrated that pure PLLA lacked bioactivity, therefore the well bioactivity was attributed to GO-HAP [11].

In order to evaluate the thermodynamic properties, TGA and DSC thermodynamic analyses were performed on the pure PLLA and PLLA/GO-HAP scaffolds as shown in Fig. 9 (a, c). It could be observed that the specimens mass remained basically stable within 250 °C, and the main mass loss stage was between 300 and 450 °C (Fig. 9(a)). The continuous weight loss in the front part of the curve for the PLLA/GO-HAP specimens was ascribed to the pyrolysis of GO [14]. In addition, it could be noted that the stable nature of the PLLA/GO-HAP scaffolds in comparison to the pure PLLA scaffolds was clarified by the DTG curves (Fig. 9(b)). The peak temperatures for the highest weight loss rate increased as the GO-

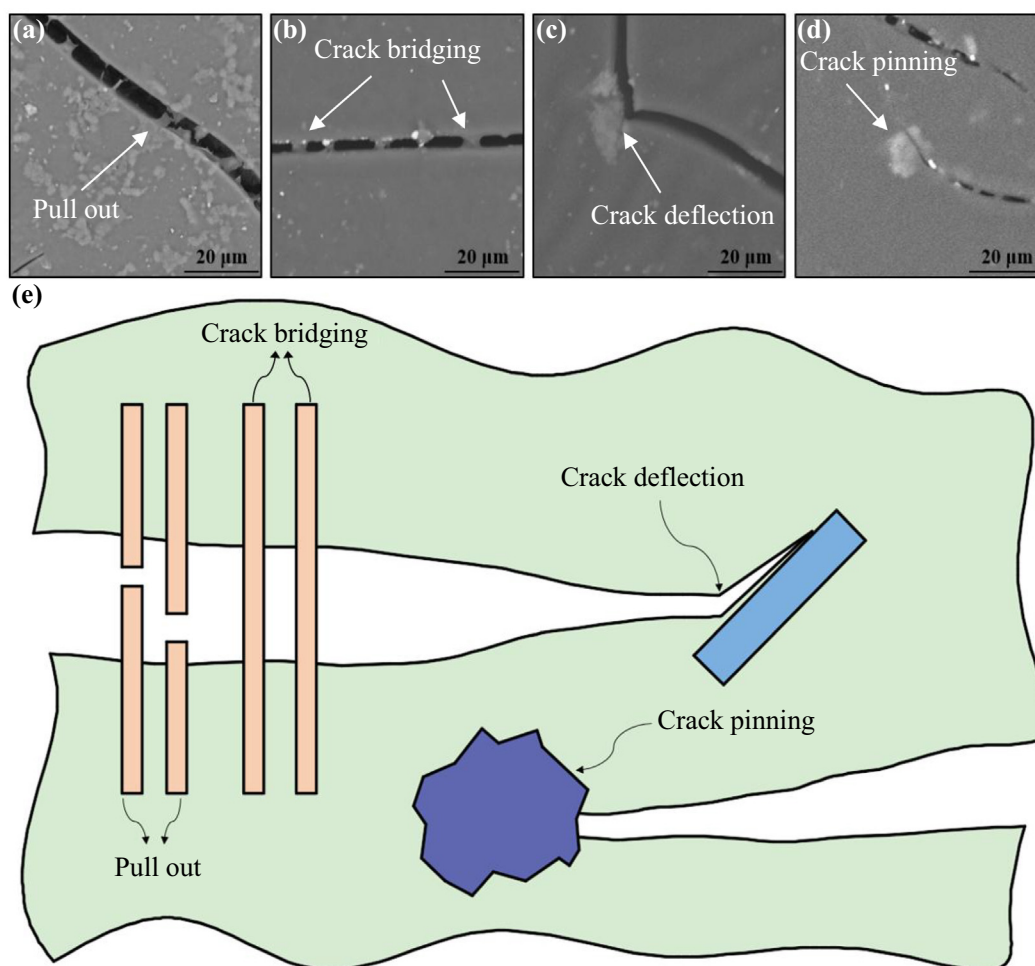


Fig. 7. SEM images of crack propagation in the PLLA/GO-HAP scaffolds including pull out (a), crack bridging (b), crack deflection (c), crack pinning (d), and the corresponding crack extension model (e).

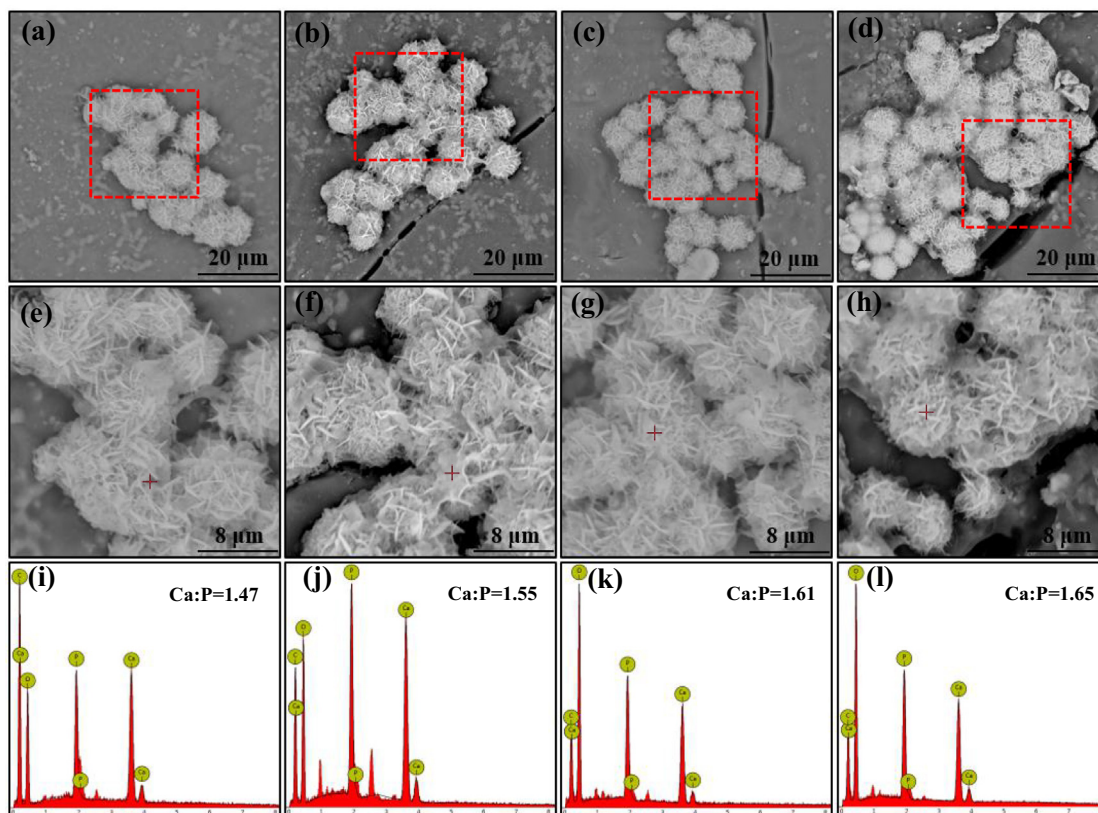


Fig. 8. The morphologies of the PLLA/GO-HAP scaffolds with 4% (a, e), 8% (b, f), 12% (c, g) and 16% (d, h) mass fractions of GO-HAP after SBF immersion for 28 d, and the corresponding EDS spectra (i-l).

HAP content in the composites was increased, indicating the introduction of GO-HAP was beneficial to the thermal stability. The DSC curves of the scaffolds were shown in Fig. 9(c). The melting temperature of the PLLA/GO-HAP specimens were 184.68 °C, 186.47 °C, 187.85 °C and 189.32 °C, respectively, which was gradually increased with the addition of GO-HAP as compared to the 183.94 °C of the pure PLLA. The maximum decomposition temperatures of the specimens were 372.04 °C, 372.88 °C, 379.47 °C, 389.85 °C and 390.30 °C, respectively. Hence, the thermal stability of PLLA was enhanced with the addition of GO-HAP, which might be ascribed to the bonding among HAP nanorods, GO nanosheets and PLLA molecules [14].

The phase compositions of the sintered scaffolds were analyzed by XRD, as presented in Fig. 9(d). It can be noted from the patterns that the two obvious Bragg diffraction peaks around at 2θ values of 16.8° and 18.9° were attributed to the (200)/(100) and (203) planes of PLLA [10]. Besides, the PLLA/GO-HAP scaffolds exhibited complete characteristic peaks of HAP. Moreover, the typical diffraction peaks of GO disappeared for several scaffolds, which was probably attributed to the relative low contents and the good dispersion of GO [14]. The wettability of the specimens was measured, as displayed in Fig. 9(e). The contact angle of the PLLA scaffold was about 83.9° which indicated the hydrophobicity of PLLA. The water contact angle of the PLLA/GO-HAP scaffolds with 4%, 8%, 12% and 16% mass fractions of GO-HAP were 74.1°, 65.9°, 58.7° and 53.6°, respectively. The decrease was ascribed to the incorporation of GO and HAP with good hydrophilicity [13]. Therefore, the scaffold presented an increase in hydrophilicity with the increasing content of GO-HAP.

Since the PLLA/12%GO-HAP scaffold exhibited the best properties in comprehensive consideration of dispersity, mechanical properties and bioactivity, it was selected for the cytocompatibility investigation of the scaffold. For this section, MG63 cells were incubated on the PLLA/12%GO-HAP scaffold for 1, 3 and 5 d. The viability of MG-63 cells on the PLLA/12%GO-HAP scaffolds was assayed after 1, 3 and 5 d of cell culture, and the fluorescence images were presented in Fig. 10(a-c). The cell after 1 d of culture showed ball-like morphologies, and the number of them increased with time. The cells extended lamellipodia and filopodia and spread well, indicating the favorable cytocompatibility of the scaffold [46,47]. Based on these images, the cell densities for different culture time were counted for accurate assessment, as shown in Fig. 10(g).

Meanwhile, the cell morphologies of different culture time were observed by SEM. It could be seen from Fig. 10(d) that MG63 cells tightly contacted with the scaffold after culturing for 1 d, presented a plump fusiform. Over time, the cells gradually became polygonal and formed extensively diffusion as shown in Fig. 10(e). The presence of the filopodia indicated the well adhesion of cells on the scaffold [48,49]. Noted from Fig. 10(f), the cells reached confluence and formed a cell layer when cultured for 5 d. Most of the area on the scaffolds were covered with cells. The adhesion area of MG63 cell on the scaffolds was calculated based on the above micrographs, as presented in Fig. 10(h). The cells spread and grew well on the scaffold, indicating the scaffold possessed favorable cytocompatibility. This was because GO and HAP possessed a positive effect on the cell adhesion, which promoted the growth and proliferation of cells [22,25].

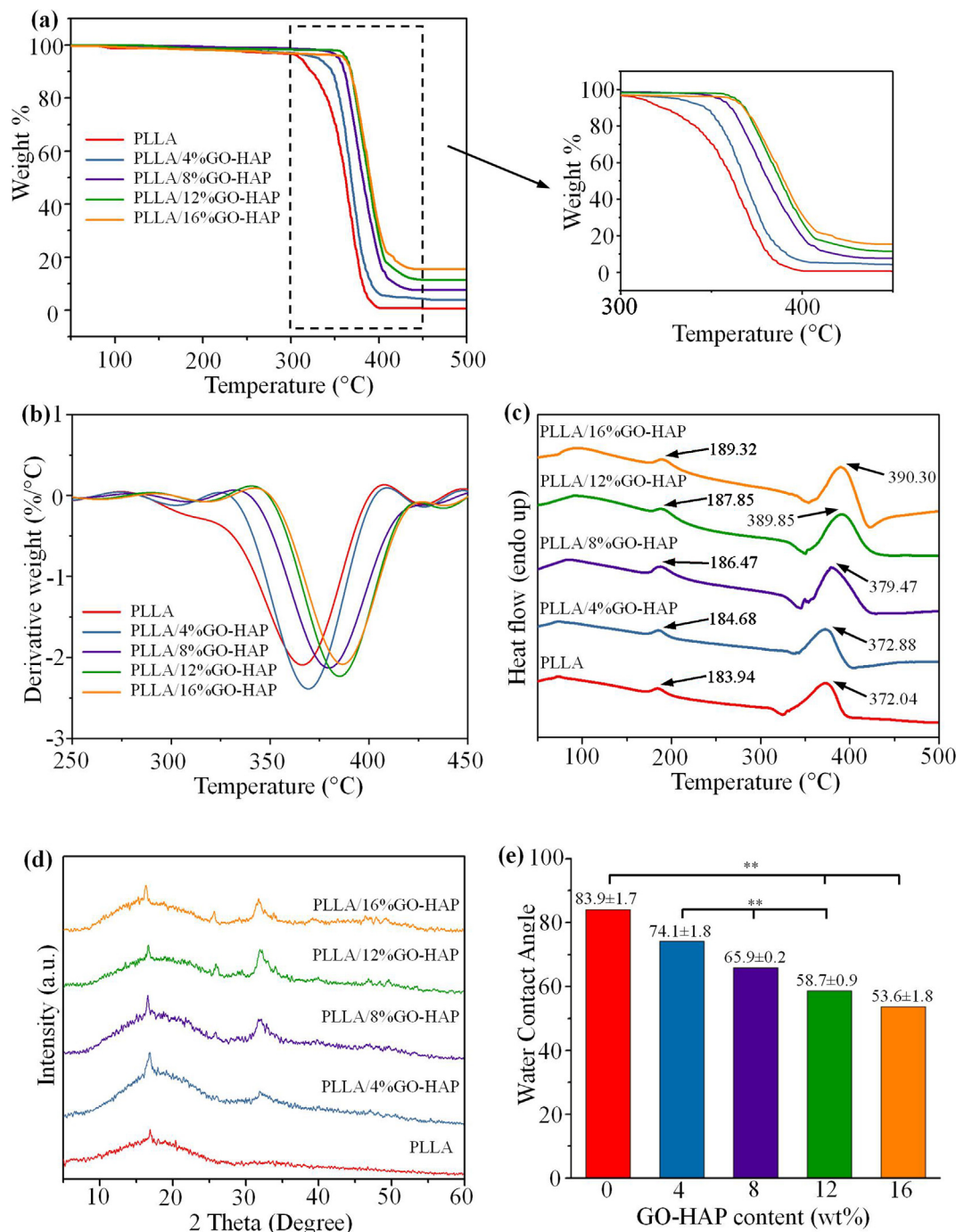


Fig. 9. The TGA spectra (a), DTG spectra (b), DSC spectra (c), XRD pattern (d) and contact angle (e) of the pure PLLA and PLLA/GO-HAP scaffolds.

Conclusions

GO-HAP nanocomposites were prepared by the in situ synthesis and introduced into PLLA, and the PLLA/GO-HAP scaffolds with good mechanical properties and bioactivity were fabricated by SLS. The GO-HAP nanocomposite presented all the functional groups and the intact crystalline structure of HAP, and the rod-like HAP nanorods were decorated uniformly on the surface and at the edges of GO nanosheets. The introduction of 12%GO-HAP greatly improved the compressive properties of the PLLA scaffold due to the pull out, crack bridging, deflection and pinning strengthening mechanisms. After being immersed in SBF solution, apatite layer with Ca/P ratio approaching 1.67 was observed on the scaffold, indicating the scaffold possessed good bioactivity. The

cytocompatibility tests indicated that the scaffold offered a good environment for adhesion, growth and proliferation of cell.

Compliance with Ethics Requirements

This article does not contain any studies with human or animal subjects.

CRediT authorship contribution statement

Cijun Shuai: Conceptualization, Supervision. **Bo Peng:** Methodology, Formal analysis, Investigation, Writing - original draft. **Pei Feng:** Conceptualization, Writing - original draft, Project adminis-

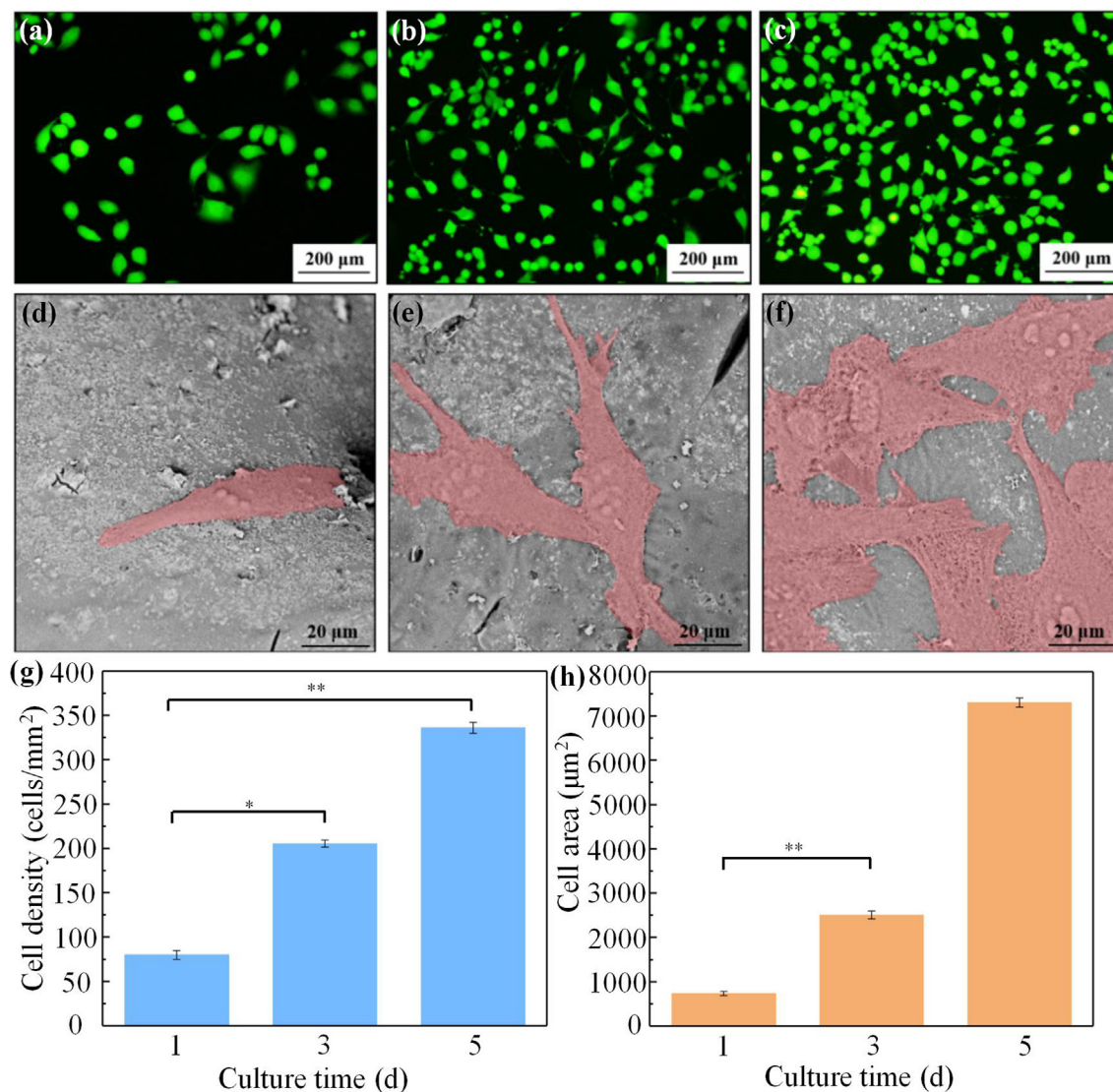


Fig. 10. The fluorescence staining of cells after culturing on the PLLA/12%GO-HAP scaffolds for 1 (a), 3 (b) and 5 (c) d, and morphology of cells after culturing on the PLLA/12%GO-HAP scaffolds for 1 (d), 3 (e) and 5 (f) d. The corresponding statistical analysis of cell densities (g) and cell area (h).

tration. **Li Yu:** Validation, Software. **Ruilin Lai:** Resources. **Anjie Min:** Data curation.

Declaration of Competing Interest

The authors declare that they have no known competing financial interests or personal relationships that could have appeared to influence the work reported in this paper.

Acknowledgements

This work was supported by the following funds: (1) The Natural Science Foundation of China (51905553, 51935014, 82072084, 81871498); (2) Hunan Provincial Natural Science Foundation of China (2019JJ50774, 2018JJ3671, 2019JJ50588, 2017JJ2392); (3) The Provincial Key R & D Projects of Jiangxi (20201BBE51012); (4) Jiangxi Provincial Natural Science Foundation of China (20192ACB20005); (5) The Project of Hunan Provincial Science and Technology Plan (2017RS3008); (6) The Project of State Key Laboratory of High Performance Complex Manufacturing, Central

South University; (7) Shenzhen Science and Technology Plan Project (JCYJ20170817112445033); (8) Technology Innovation Platform Project of Shenzhen Institute of Information Technology 2020 (PT2020E002); (9) Scientific research project of Hunan provincial health commission (B20180054); (10) Changsha science and technology project (kq1706072).

References

- [1] Ambekar RS, Kandasubramanian B. Progress in the advancement of porous biopolymer scaffold: tissue engineering application. *Ind Eng Chem Res* 2019;58(16):6163–94.
- [2] Murphy SV, De Coppi P, Atala A. Opportunities and challenges of translational 3D bioprinting. *Nat Biomed Eng* 2020;4(4):370–80.
- [3] Kaviyarasu K, Manikandan E, Kennedy J, Maaza M. Synthesis and analytical applications of photoluminescent carbon nanosheet by exfoliation of graphite oxide without purification. *J Mater Sci-Mater El* 2016;27(12):13080–5.
- [4] Baradaran S, Moghaddam E, Basirun WJ, Mehrali M, Sookhakistan M, Hamdi M, et al. Mechanical properties and biomedical applications of a nanotube hydroxyapatite-reduced graphene oxide composite. *Carbon* 2014;69:32–45.
- [5] Ramadas M, Bharath G, Ponpandian N, Ballamurugan AM. Investigation on biophysical properties of Hydroxyapatite/Graphene oxide (HAp/GO) based binary nanocomposite for biomedical applications. *Mater Chem Phys* 2017;199:179–84.

